ON THE DESIGN OF NON-(BI)ORTHOGONAL PULSE-SHAPED FDM FOR DOUBLY-DISPERSIVE CHANNELS

Philip Schniter

Dept. EE, The Ohio State University, 2015 Neil Ave, Columbus, OH 43210
schniter.1@osu.edu

ABSTRACT

We consider the design of max-SINR pulse-shaped (PS) frequency domain modulation (FDM), where signal to interference-plus-noise ratio (SINR) is defined in accordance with inter-symbol and inter-carrier interference (ISI/ICI) shaping rather than complete ISI/ICI suppression. Because the transmitter is assumed to know the channel scattering function but not the channel realization, the resulting max-SINR pulses are non-(bi)orthogonal. For this case, numerical results suggest that max-SINR systems designed for ISI/ICI-shaping achieve higher outage capacity than those designed for ISI/ICI-suppression. An outage capacity analysis is also used to obtain rough design guidelines for max-SINR non-(bi)orthogonal PS-FDM, since the design paradigm differs from that of (bi)orthogonal PS-FDM.

1. INTRODUCTION

The design of pulse-shaped (PS) frequency-domain modulation (FDM) systems for doubly-selective channels has been considered by many authors (e.g., [1–8]). These works assume a linear modulation/demodulation structure in that finite-alphabet symbols $\{s_{k,l}\}$ are modulated onto time-frequency translated pulses $\{a_{k,l}(t)\}$ and demodulated using inner products between the (noisy, spread) received signal and the time-frequency translated pulses $\{b_{k,l}(t)\}$. Orthogonal systems are those with $b_{k,l}(t) = a_{k,l}(t)$ and $\langle a_{k,l}(t), a_{m,n}(t)\rangle = \delta_{k-m}\delta_{l-n}$, while biorthogonal systems are those with $\langle a_{k,l}(t), b_{m,n}(t)\rangle = \delta_{k-m}\delta_{l-n}$. (Bi)orthogonal systems have the elegant property that inter-symbol interference (ISI) and inter-carrier interference (ICI) are absent in non-dispersive environments, though they suffer from ISI/ICI when used in dispersive environments. While some authors have assumed that this interference is negligible (e.g., [5]), appealing to the existence of an "approximate" eigen-basis for underspread channels [9], others have investigated the design of pulse prototypes $a_{0,0}(t)$ and $b_{0,0}(t)$ which minimize the interference energy for a given delay/Doppler spread under (bi)orthogonality constraints (e.g., [4, 6, 7]). (Bi)orthogonal PS-FDM systems are, however, capable of significant interference suppression only when designed with spectral efficiencies less[1] than 0.8. (See, e.g., the discussion in [7].)

The PS-FDM system proposed by the author in [11] is a significant departure from the previously cited literature in that the pulses are designed to *allow* ISI/ICI within a target pattern. The target pattern is chosen so that the residual ISI/ICI can be resolved by a high-performance, yet low-complexity, soft interference cancellation (IC) algorithm. Pulse prototypes are then designed to minimize out-of-target ISI/ICI given knowledge of the channel fading statistics (i.e., the scattering function [12]). Clearly, this system is non-(bi)orthogonal. Thus, [11] advocates ISI/ICI *shaping* rather than ISI/ICI suppression.

When ISI/ICI is permitted, many of the standard OFDM system design rules must be reconsidered. For example, it is no longer the case that the cyclic prefix length must be greater than channel delay spread. Similarly, the FDM symbol duration does not need to be less than the channel coherence time. In addition, new questions arise. What is the optimal target ISI/ICI pattern? Should we design for unit spectral efficiency? In an attempt to answer these questions, we examine the outage capacity [13] of the non-(bi)orthogonal PS-FDM system [11] for various design choices.

Notation: We use $(\cdot)^t$ to denote transpose, $(\cdot)^*$ conjugate, and $(\cdot)^H$ conjugate transpose. $\boldsymbol{I}$ denotes the identity matrix, and $[\boldsymbol{B}]_{m,n}$ denotes the element in the m^{th} row and n^{th} column of $\boldsymbol{B}$, where row/column indices begin with zero. $\odot$ denotes the Hadamard product, $\mathrm{E}\{\cdot\}$ expectation, δ_m the Kronecker delta, and $\mathbb{Z}$ the set of integers.

2. SYSTEM MODEL

At each $i \in \mathbb{Z}$, a set of N coded QAM symbols $\{s_k^{(i)}\}$ is collected to form a FDM symbol $\boldsymbol{s}^{(i)} = [s_0^{(i)}, \ldots, s_{N-1}^{(i)}]^t$. These symbols are used to modulate pulsed carriers as follows:

$$t_n \;=\; \sum_{i=-\infty}^{\infty} a_{n-iN_s} \frac{1}{\sqrt{N}} \sum_{k=0}^{N-1} s_k^{(i)} e^{j\frac{2\pi}{N}(n-iN_s-N_o)k} \qquad (1)$$

In (1), $\{a_n\}$ is the transmit pulse sequence, N_s is the FDM symbol interval, and $N_o \in \{0, \ldots, N-1\}$ delays the carrier origin relative to the pulse origin. The multipath channel is described by its time-variant discrete impulse response $h_{\text{tl}}(n, l)$, defined as the time-n response to an impulse applied at time $n-l$. We assume a causal impulse response of length of N_h. The signal observed by the receiver is then

$$r_n \;=\; \nu_n + \sum_{l=0}^{N_h-1} h_{\text{tl}}(n, l) t_{n-l} \qquad (2)$$

where ν_n denotes samples of additive white circular Gaussian noise (AWGN) with variance σ^2. Defining $r_n^{(i)} := r_{iN_s+n}$, $\nu_n^{(i)} :=$

This work is supported in part by NSF CAREER Grant CCR-0237037.

[1] A different technique, OFDM-OQAM, is said to yield good ISI/ICI suppression with unit spectral efficiency [10]. The implementation complexity of these systems is substantially greater than that of PS-FDM, however, and rises in proportional to their ISI/ICI suppression capabilities.

ν_{iN_s+n}, and $h_{\mathsf{tl}}^{(i)}(n,l) := h_{\mathsf{tl}}(iN_s+n,l)$, we find

$$r_n^{(i)} = \nu_n^{(i)} + \sum_{l=0}^{N_h-1} h_{\mathsf{tl}}^{(i)}(n,l) \sum_{\ell=-\infty}^{\infty} a_{\ell N_s+n-l} \times \frac{1}{\sqrt{N}} \sum_{k=0}^{N-1} s_k^{(i-\ell)} e^{j\frac{2\pi}{N}(n-l+\ell N_s-N_o)k} \quad (3)$$

To estimate the FDM symbol $\boldsymbol{s}^{(i)}$, the receiver employs the pulse $\{b_n\}$ as follows:

$$x_d^{(i)} = \frac{1}{\sqrt{N}} \sum_n r_n^{(i)} b_n e^{-j\frac{2\pi}{N}d(n-N_o)} \quad (4)$$

Here again N_o delays the carrier origin relative to the pulse origin. Note that this system reduces to CP-OFDM with $N_o = N_s - N$, $\{a_n\}_{n=0}^{N_s-1} = 1$, and $\{b_n\}_{n=N_o}^{N_s-1} = 1$ (else $a_n = b_n = 0$). Note also that $N_g := N_s - N$ is analogous to CP-OFDM guard interval length, though in PS-FDM we allow $N_g < 0$.

Plugging (3) into (4), we find

$$x_d^{(i)} = w_d^{(i)} + \sum_{\ell} \sum_{k=0}^{N-1} \breve{h}_{\mathsf{df}}^{(i,\ell)}(d-k,k)\, s_k^{(i-\ell)} \quad (5)$$

where

$$w_d^{(i)} := \frac{1}{\sqrt{N}} \sum_n b_n \nu_n^{(i)} e^{-j\frac{2\pi}{N}d(n-N_o)} \quad (6)$$

$$\breve{h}_{\mathsf{df}}^{(i,\ell)}(d,k) := \frac{1}{N} \sum_n \sum_{l=0}^{N_h-1} h_{\mathsf{tl}}^{(i)}(n,l) b_n a_{\ell N_s+n-l} \times e^{-j\frac{2\pi}{N}d(n-N_o)} e^{-j\frac{2\pi}{N}k(l-\ell N_s)} \quad (7)$$

Equation (5) indicates that $\breve{h}_{\mathsf{df}}^{(i,\ell)}(d,k)$ can be interpreted as the response, at time i and subcarrier $k+d$, to a frequency-domain impulse applied at time $i-\ell$ and subcarrier k. In practice we implement finite-duration causal pulses $\{a_n\}$ and $\{b_n\}$ of length N_a and N_b, respectively, implying that $\breve{h}_{\mathsf{df}}^{(i,\ell)}(d,k)$ is non-zero only for $\ell \in \{-L_{\mathsf{pre}}, \ldots, L_{\mathsf{pst}}\}$ where $L_{\mathsf{pre}} = -\lfloor \frac{N_b-1}{N_s} \rfloor$ and $L_{\mathsf{pst}} = \lfloor \frac{N_a+N_h-2}{N_s} \rfloor$. (See [11] for details.)

With the definitions $\boldsymbol{x}^{(i)} := [x_0^{(i)}, \ldots, x_{N-1}^{(i)}]^t$, $\boldsymbol{w}^{(i)} := [w_0^{(i)}, \ldots, w_{N-1}^{(i)}]^t$, and $[\mathcal{H}^{(i,\ell)}]_{d,k} := \breve{h}_{\mathsf{df}}^{(i,\ell)}(d-k,k)$, (5) implies the linear time-varying (LTV) multiple-input multiple-output (MIMO) system

$$\boldsymbol{x}^{(i)} = \boldsymbol{w}^{(i)} + \sum_{\ell=-L_{\mathsf{pre}}}^{L_{\mathsf{pst}}} \mathcal{H}^{(i,\ell)} \boldsymbol{s}^{(i-\ell)}. \quad (8)$$

In the sequel we assume wide-sense stationary uncorrelated scattering (WSSUS) [12] so that $\mathrm{E}\{h_{\mathsf{tl}}(n,l)h_{\mathsf{tl}}^*(n-q,l-m)\} = r_{\mathsf{t}}(q)\sigma_l^2\delta_m$ with $r_{\mathsf{t}}(q)$ denoting normalized autocorrelation (i.e., $r_{\mathsf{t}}(0) = 1$) and σ_l^2 the variance of the l^{th} lag. We also assume zero-mean symbols such that $\mathrm{E}\{\boldsymbol{s}^{(i)}\boldsymbol{s}^{(i-\ell)H}\} = \boldsymbol{I}\delta_\ell$.

3. PULSE DESIGN

The choice of $\{a_n\}$ and $\{b_n\}$ affect the ISI/ICI patterns of the MIMO system (8). For example, it is well known that the CP-OFDM choices yield an system for which ISI and ICI vanish *if* the channel is LTI with delay spread $N_h \leq N_g + 1$. The absence of ISI/ICI greatly simplifies detection; this is the classical motivation for CP-OFDM and, more generally, (bi)orthogonal PS-FDM. When the channel is LTV or it is impractical to enforce $N_h \leq N_s - N + 1$, however, no choice of $\{a_n\}$ and $\{b_n\}$ is capable of completely suppressing both ISI and ICI. We advocate the design of pulses which impart a particular structure on the effective channel response $\mathcal{H}^{(i,\ell)}$. A good target ISI/ICI pattern should allow high-performance/low-complexity detection *while being nearly attainable for some choice of* $\{a_n\}$ *and* $\{b_n\}$; when the channel is significantly dispersive, a target which suppresses all ISI/ICI (e.g., [4, 7, 8]) may not be attainable.

The lowpass nature of Doppler spectra typically encountered in wireless communication implies that ICI will be strongest from neighboring carriers. In other words, for smooth (or rectangular) pulse shapes, the "cursor" coefficient $\mathcal{H}^{(i,0)}$ will have large entries in near the main diagonal and smaller entries elsewhere. (See [14] for an ICI analysis with CP-OFDM pulses.) With well designed pulses, the ISI coefficients $\{\mathcal{H}^{(i,\ell)}\}_{\ell\neq 0}$ can be made small relative to the ICI response when the delay spread is less[2] than the FDM symbol length [11]. These observations motivate an ICI/ISI target in which $\{\mathcal{H}^{(i,\ell)}\}_{\ell\neq 0}$ equal zero and $\mathcal{H}^{(i,0)}$ has the banded structure illustrated by Fig. 1 for some integer D. The choice of D is discussed in the sequel.

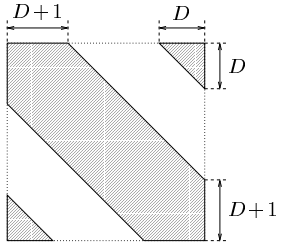

Fig. 1. Desired structure of MIMO cursor coefficient $\mathcal{H}^{(i,0)}$.

In [11] we proposed pulse designs which maximized SINR := $\mathcal{E}_s/\mathcal{E}_{ni}$, where signal energy $\mathcal{E}_s$ and noise-plus-interference energy $\mathcal{E}_{ni}$ are defined relative to the target. If we define $\mathcal{E}_{\mathsf{s},d}$ to be the energy contributed by $s_d^{(i)}$ to $x_d^{(i)}$, and if we define $\mathcal{E}_{\mathsf{ni},d}$ to be the energy contributed to $x_d^{(i)}$ by additive noise $w_d^{(i)}$, non-cursor symbols $\{s_d^{(j)}\}_{j\neq i}$, and non-neighboring co-cursor symbols $\{s_k^{(i)}\}_{k=0}^{d-D-1} \cup \{s_k^{(i)}\}_{k=d+D+1}^{N-1}$, then $\mathcal{E}_s = \sum_d \mathcal{E}_{\mathsf{s},d}$ and $\mathcal{E}_{ni} = \sum_d \mathcal{E}_{\mathsf{ni},d}$. Note that the energy contributed to $x_d^{(i)}$ by neighboring co-cursor symbols $\{s_k^{(i)}\}_{k=d-D}^{d-1} \cup \{s_k^{(i)}\}_{k=d+1}^{d+D}$ is considered neither signal nor interference, but rather a "don't care" quantity. In choosing $\boldsymbol{a} := [a_0, \ldots, a_{N_a-1}]^t$, we impose the average transmitted power constraint $\|\boldsymbol{a}\|^2 = N_s$. Since the norm of the receive pulse $\boldsymbol{b} := [b_0, \ldots, b_{N_b-1}]^t$ is inconsequential (i.e., signal, noise, and interference scale together), we can choose $\|\boldsymbol{b}\|^2 = N_s$ without loss of generality.

3.1. Max-SINR Pulses

It was shown in [11] that alternating the pair (9)-(10) jointly optimizes SINR with respect to $\boldsymbol{a}$ and $\boldsymbol{b}$ under the constraints $\|\boldsymbol{a}\|^2 =$

[2] If the delay spread is long compared to the FDM symbol interval, block decision feedback detection may be applied, in which case the pulses should be designed to allow arbitrary post-cursor ISI. For details see [11].

$\|\boldsymbol{b}\|^2 = N_s$. We use $\boldsymbol{v}_\star(\boldsymbol{M},\boldsymbol{N})$ to denote the principle generalized eigenvector of the matrix pair $(\boldsymbol{M},\boldsymbol{N})$.

$$\boldsymbol{b}_{\star|\boldsymbol{a}} \;=\; \sqrt{N_s}\cdot \boldsymbol{v}_\star\big(\boldsymbol{R}_b \odot \boldsymbol{A}_{\mathsf{s}},\; \sigma^2\boldsymbol{I} + \boldsymbol{R}_b\odot\boldsymbol{C}_b\odot\boldsymbol{A}_{\mathsf{t}} - \boldsymbol{R}_b\odot\boldsymbol{D}_b\odot\boldsymbol{A}_{\mathsf{s}}\big) \quad (9)$$

$$\boldsymbol{a}_{\star|\boldsymbol{b}} \;=\; \sqrt{N_s}\cdot \boldsymbol{v}_\star\big(\boldsymbol{R}_a \odot \boldsymbol{B}_{\mathsf{s}},\; \sigma^2\boldsymbol{I} + \boldsymbol{R}_a\odot\boldsymbol{C}_a\odot\boldsymbol{B}_{\mathsf{t}} - \boldsymbol{R}_a\odot\boldsymbol{D}_a\odot\boldsymbol{B}_{\mathsf{s}}\big) \quad (10)$$

The matrices in (9) are $N_b \times N_b$ and defined element-wise as $[\boldsymbol{R}_b]_{m,n} := r_{\mathsf{t}}(n-m)$, $[\boldsymbol{A}_{\mathsf{s}}]_{m,n} := \sum_{l=0}^{N_h-1}\sigma_l^2 a_{n-l}a^*_{m-l}$, $[\boldsymbol{C}_b]_{m,n} := \delta(\langle n-m\rangle_N)$, $[\boldsymbol{D}_b]_{m,n} := \frac{1}{N}\sin(\frac{\pi}{N}(2D+1)(n-m))/\sin(\frac{\pi}{N}(n-m))$, and $[\boldsymbol{A}_{\mathsf{t}}]_{m,n} := \sum_{\ell=-L_{\mathsf{pre}}}^{L_{\mathsf{pst}}}\sum_{l=0}^{N_h-1}\sigma_l^2 a_{\ell N_s+n-l}a^*_{\ell N_s+m-l}$. The matrices in (10) are $N_a \times N_a$ and defined element-wise as $[\boldsymbol{R}_a]_{p,q} := r_{\mathsf{t}}(q-p)$, $[\boldsymbol{B}_{\mathsf{s}}]_{p,q} := \sum_{l=0}^{N_h-1}\sigma_l^2 b_{q+l}b^*_{p+l}$, $[\boldsymbol{D}_a]_{p,q} := \frac{1}{N}\sin(\frac{\pi}{N}(2D+1)(q-p))/\sin(\frac{\pi}{N}(q-p))$, $[\boldsymbol{B}_{\mathsf{t}}]_{p,q} := \sum_{\ell=-L_{\mathsf{pre}}}^{L_{\mathsf{pst}}}\sum_{l=0}^{N_h-1}\sigma_l^2 b_{q+l-\ell N_s}b^*_{p+l-\ell N_s}$, and $[\boldsymbol{C}_a]_{p,q} := \delta(\langle q-p\rangle_N)$. We note that (9)-(10) must be alternated because $\boldsymbol{A}_{\mathsf{s}}$ and $\boldsymbol{A}_{\mathsf{t}}$ are functions of $\boldsymbol{a}$ and $\boldsymbol{B}_{\mathsf{s}}$ and $\boldsymbol{B}_{\mathsf{t}}$ are functions of $\boldsymbol{b}$. In the case of Rayleigh fading, we note that the pulses designs depend only on maximum Doppler frequency, power profile, and noise variance.

While (9)-(10) is only guaranteed to converge to a local SINR maximum, our experience leads us to believe that the global maximum is obtained from a properly chosen initialization (e.g., the Gaussian pulses discussed below). In practice, (9)-(10) could be carried out in advance for particular fading scenarios and the resulting pulses stored at the terminals.

3.2. SINR-Maximizing Gaussian Pulses

It is well known that the Gaussian pulse has the best time-frequency localization among all pulses. Thus, several authors have considered its use for PS-FDM (e.g., [8, 15]). Adapting the Gaussian pulse to our system, we employ the SINR-maximizing parameters $\{\mu_a,\sigma_a,\mu_b,\sigma_b\}$ in the finite-length pulses (11)-(12), noting $\|\boldsymbol{a}\|^2 = \|\boldsymbol{b}\|^2 = N_s$,

$$a_n \;=\; \sqrt{N_s}(2\pi\sigma_a^2)^{-\frac{1}{4}}e^{-\frac{(n-\mu_a)^2}{4\sigma_a^2}},\; n\in\{0\ldots N_a-1\} \quad (11)$$

$$b_n \;=\; \sqrt{N_s}(2\pi\sigma_b^2)^{-\frac{1}{4}}e^{-\frac{(n-\mu_b)^2}{4\sigma_b^2}},\; n\in\{0\ldots N_b-1\} \quad (12)$$

via numerical optimization of (13) (which was derived in [11]).

$$\text{SINR} \;=\; \frac{\boldsymbol{b}^H\big(\boldsymbol{R}_b\odot\boldsymbol{A}_{\mathsf{s}}\big)\boldsymbol{b}}{\boldsymbol{b}^H\big(\sigma^2\boldsymbol{I}+\boldsymbol{R}_b\odot\boldsymbol{C}_b\odot\boldsymbol{A}_{\mathsf{t}}-\boldsymbol{R}_b\odot\boldsymbol{D}_b\odot\boldsymbol{A}_{\mathsf{s}}\big)\boldsymbol{b}} \quad (13)$$

4. OUTAGE ANALYSIS

To predict PS-FDM performance with a practical coding scheme (i.e., finite decoding delay), we examine outage capacity. It is assumed that bits are coded across a block of M FDM symbols and, for simplicity, that the entries in $\boldsymbol{s}^{(i)}$ are circular Gaussian. As an example, consider $M=2$, $L_{\mathsf{pre}}=1$, and $L_{\mathsf{pst}}=2$. Equation (8) implies the block system model (14) at block index $j=0$:

$$\begin{bmatrix}\boldsymbol{x}^{(1)}\\ \boldsymbol{x}^{(0)}\end{bmatrix} = \begin{bmatrix}\mathcal{H}^{(1,0)} & \mathcal{H}^{(1,1)}\\ \mathcal{H}^{(0,-1)} & \mathcal{H}^{(0,0)}\end{bmatrix}\begin{bmatrix}\boldsymbol{s}^{(1)}\\ \boldsymbol{s}^{(0)}\end{bmatrix} + \begin{bmatrix}\boldsymbol{w}^{(1)}\\ \boldsymbol{w}^{(0)}\end{bmatrix} + \left[\begin{array}{c|cc}\mathcal{H}^{(1,-1)} & \mathcal{H}^{(1,2)} & \boldsymbol{0}\\ \boldsymbol{0} & \mathcal{H}^{(0,1)} & \mathcal{H}^{(0,2)}\end{array}\right]\left[\begin{array}{c}\boldsymbol{s}^{(2)}\\ \hline \boldsymbol{s}^{(-1)}\\ \boldsymbol{s}^{(-2)}\end{array}\right]. \quad (14)$$

Note that the last two terms in (14) constitute noise and pre/post-cursor interference, respectively. More generally, we define $\underline{\boldsymbol{x}}^{(j)} := [\boldsymbol{x}^{(Mj+M-1)t},\ldots,\boldsymbol{x}^{(Mj)t}]^t$ and $\underline{\boldsymbol{s}}^{(j)} := [\boldsymbol{s}^{(Mj+M-1)t},\ldots,\boldsymbol{s}^{(Mj)t}]^t$, and we construct the matrix $\mathcal{H}^{(j)}$ with M block rows and M block columns, where the $(k,l)^{th}$ block equals $\mathcal{H}^{(Mj+M-1-k,l-k)}$. Finally, we collect the noise and pre/post-cursor contributions into the Gaussian vector $\underline{\boldsymbol{v}}^{(j)}\in\mathbb{C}^{MN}$, yielding the block system model $\underline{\boldsymbol{x}}^{(j)} = \mathcal{H}^{(j)}\underline{\boldsymbol{s}}^{(j)} + \underline{\boldsymbol{v}}^{(j)}$. We denote $\boldsymbol{R}_v := \mathrm{E}\{\underline{\boldsymbol{v}}^{(j)}\underline{\boldsymbol{v}}^{(j)H}\}$.

The mutual information between $\underline{\boldsymbol{s}}^{(j)}$ and $\underline{\boldsymbol{x}}^{(j)}$, in bits per channel use, is given by

$$\mathcal{I}_M^{(j)} \;=\; \frac{1}{MN_s}\log_2\det\big(\boldsymbol{I}_{MN}+\mathcal{H}^{(j)H}\boldsymbol{R}_v^{-1}\mathcal{H}^{(j)}\big), \quad (15)$$

Since $\mathcal{H}^{(j)}$ is random, so is $\mathcal{I}_M^{(j)}$. The P_o-outage capacity C_o is defined through the relationship $P_o = \Pr\{I_M^{(j)} < C_o\}$. Our experiments indicate that $I_M^{(j)}$ is well modeled by the normal r.v. $\mathcal{N}(\mu,\sigma^2)$, in which case it is straightforward to show that

$$C_o \;=\; \mu + \sigma\,\mathrm{erfinv}(2P_o-1). \quad (16)$$

To compute C_o for the plots in Sec. 5, we use (16) with $\{\mu,\sigma\}$ estimated from 1000 realizations of $\mathcal{I}_M^{(j)}$.

Recall that the pulses in Sec. 3.1 and Sec. 3.2 were designed for efficient detection—not for maximum C_o. However, outage analysis can be used to choose the values $\{N,D,N_g\}$ used in pulse construction and to predict overall performance.

5. NUMERICAL RESULTS AND DISCUSSION

All experiments employ SNR^{-1}-variance circular AWGN $\{\nu_n\}$, a WSSUS Rayleigh-fading channel with $\sigma_l^2 = N_h^{-1}$ (for $0\le l\le N_h$) and $N_h=8$, and pulse lengths $N_a = 1.5N_s$ and $N_b = N_a + \lceil Nh/2\rceil$. Bits are coded across 64 scalar symbols $\{s_k^{(i)}\}$, so that $M = 64/N$, allowing a fair comparison among different choices of N. "PS-FDM" refers to the power-constrained max-SINR pulses of Sec. 3.1, while "GP-FDM" refers to the power/Gaussian-constrained max-SINR pulses of Sec. 3.2. Recall that f_{d} is Doppler normalized to the *channel-use* interval rather than the FDM-symbol interval.

Figure 2 shows typical traces of C_o versus Nf_{d} for various D. Here we use GP-FDM with unit spectral efficiency (i.e., $N_g=0$). Notice that C_o-maximization occurs at $D\approx Nf_{\mathsf{d}}$. Since $D=0$ is optimum only for relatively small Nf_{d}, we conclude that, *for roughly $Nf_{\mathsf{d}}>1$, target responses allowing ICI are advantageous from an outage capacity standpoint*.

Figure 3 plots C_o versus f_{d} for various SNRs and FFT size N. In all cases the C_o-maximizing choice of D was employed. PS-FDM performs equivalently to GP-FDM at the shortest FFT size ($N=8$). As N increases, the capacity of PS-FDM increases slightly while the capacity of GP-FDM decreases slightly (and significantly at $N=64$.). We attribute this to the lack of freedom in GP-FDM, relative to PS-FDM, pulse design. Note that, when D and N are well chosen, capacity increases with f_{d} (a consequence of Doppler diversity).

Figure 4 plots C_o versus f_{d} for various values of N and "equivalent guard interval" N_g. Note $N_g = \{-\frac{N}{4},0,\frac{N}{4}\}$ correspond to spectral efficiencies $\{\frac{4}{3},1,\frac{4}{5}\}$, respectively; $N_g<0$ yields an *overloaded* system which transmits >1 symbol per channel use (on average). The results suggest a small C_o *gain from overloading* and a more significant C_o loss for spectral efficiencies <1 (irrespective of N and f_{d}). Clearly, overloading is possible only with non-(bi)orthogonal signaling.

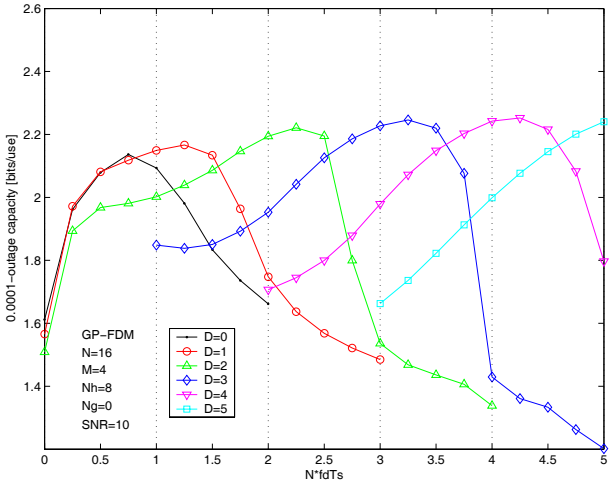

Fig. 2. Prototypical C_o versus Nf_{d} for various D.

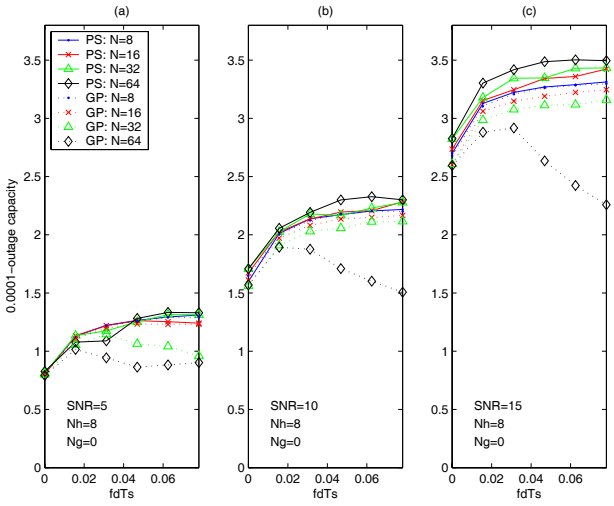

Fig. 3. C_o versus f_{d} for various SNRs and FFT size N.

6. CONCLUSIONS

The outage capacity C_o of max-SINR PS-FDM was examined, where SINR was defined according to a target pattern which allows ICI from $2D$ adjacent subcarriers. Numerical results suggest that capacity is maximized for $D \approx Nf_{\mathsf{d}}$, implying that ICI/ISI-free designs (i.e., $D = 0$) are appropriate for small values of Nf_{d}, while ICI-tolerating designs (i.e., $D > 0$) are more appropriate for larger values of Nf_{d}. The choice of FFT size and spectral efficiency were also examined.

7. REFERENCES

[1] R. W. Chang, "Synthesis of band-limited orthogonal signals for multi-channel data transmission," *Bell System Tech. J.*, vol. 45, pp. 1775–1796, Dec. 1966.

[2] B. Le Floch, M. Alard, and C. Berrou, "Coded orthogonal frequency division multiplex," *Proc. IEEE*, vol. 83, pp. 982–996, June 1995. 1995.

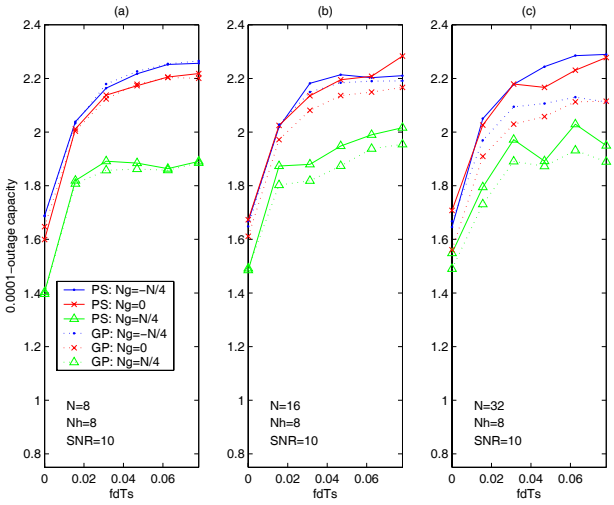

Fig. 4. C_o versus f_{d} for various FFT sizes N and "guards" $N_g = N_s - N$.

[3] R. Haas and J.-C. Belfiore, "A time-frequency well-localized pulse for multiple carrier transmission," *Wireless Personal Commun.*, vol. 5, pp. 1–18, 1997.

[4] W. Kozek and A. F. Molisch, "Nonorthogonal pulseshapes for multicarrier communications in doubly dispersive channels," *IEEE J. Select. Areas In Commun.*, vol. 16, pp. 1579–1589, Oct. 1998.

[5] H. Bölcskei, R. Koetter, and S. Mallik, "Coding and modulation for underspread fading channels," in *Proc. IEEE Int. Symposium Inform. Theory*, p. 358, June 2002.

[6] D. Schaufhuber, G. Matz, and F. Hlawatsch, "Pulse-shaping OFDM/BFDM systems for time-varying channels: ISI/ICI analysis, optimal pulse design, and efficient implementation," in *Proc. IEEE Symp. PIMRC*, pp. 1012–1016, Sep. 2002.

[7] T. Strohmer and S. Beaver, "Optimal OFDM design for time-frequency dispersive channels," *IEEE Trans. Commun.*, to appear.

[8] K. Liu, T. Kadous, and A. M. Sayeed, "Orthogonal time-frequency signaling over doubly dispersive channels," *IEEE Trans. Inform. Theory*, to appear.

[9] W. Kozek, *Matched Weyl-Heisenberg Expansions of Nonstationary Environments*. PhD thesis, Vienna Univ. of Technology, March 1997.

[10] H. Bölcskei, "Orthogonal frequency division multiplexing based on offset QAM," in *Advances in Gabor Theory* (H. G. Feichtinger and T. Strohmer, eds.), Birkhäuser, 2002.

[11] P. Schniter, "A new approach to multicarrier pulse design for doubly-dispersive channels," in *Proc. Allerton Conf. Commun., Control, and Computing*, Oct. 2003.

[12] J. G. Proakis, *Digital Communications*. New York: McGraw-Hill, 4th ed., 2001.

[13] L. H. Ozarow, S. Shamai, and A. D. Wyner, "Information theoretic constraints for cellular mobile radio," *IEEE Trans. Veh. Tech.*, vol. 43, pp. 359–378, May 1994.

[14] P. Schniter, "Low-complexity equalization of OFDM in doubly-selective channels," *IEEE Trans. Signal Processing*. (to appear).

[15] K. Matheus and K.-D. Kammeyer, "Optimal design of a multicarrier systems with soft impulse shaping including equalization in time or frequency direction," in *IEEE Globecom*, vol. 1, pp. 310–314, 1997.